Review of
Scientific Instruments

RESEARCH ARTICLE | NOVEMBER 16 2022

Design elements and first data from a new Doppler backscattering system on the MAST-U spherical tokamak

FREE

Special Collection: Proceedings of the 24th Topical Conference on High-Temperature Plasma Diagnostics

T. L. Rhodes; C. A. Michael; P. Shi; R. Scannell; S. Storment; Q. Pratt; R. Lantsov; I. Fitzgerald; V. H. Hall-Chen; N. A. Crocker; W. A. Peebles

Rev. Sci. Instrum. 93, 113549 (2022)
https://doi.org/10.1063/5.0101848

Review of Scientific Instruments | ARTICLE | scitation.org/journal/rsi

Design elements and first data from a new Doppler backscattering system on the MAST-U spherical tokamak

Cite as: Rev. Sci. Instrum. 93, 113549 (2022); doi: 10.1063/5.0101848
Submitted: 3 June 2022 • Accepted: 25 September 2022 •
Published Online: 16 November 2022

View Online | Export Citation | CrossMark

T. L. Rhodes,[1,a)] C. A. Michael,[1] P. Shi,[2] R. Scannell,[2] S. Storment,[1] Q. Pratt,[1] R. Lantsov,[1] I. Fitzgerald,[2] V. H. Hall-Chen,[3] N. A. Crocker,[1] and W. A. Peebles[1]

AFFILIATIONS

[1] Physics and Astronomy Department, University of California, Los Angeles, California 90098, USA
[2] UKAEA/CCFE, Culham Science Centre, Abingdon, Oxfordshire, OX14 3DB, UK
[3] Institute of High Performance Computing, Singapore 138632, Singapore

Note: This paper is part of the Special Topic on Proceedings of the 24th Topical Conference on High-Temperature Plasma Diagnostics.

[a)] **Author to whom correspondence should be addressed:** trhodes@ucla.edu

ABSTRACT

A new Doppler backscattering (DBS) system has been installed and tested on the MAST-U spherical tokamak. It utilizes eight simultaneous fixed frequency probe beams (32.5, 35, 37.5, 40, 42.5, 45, 47.5, and 50 GHz). These frequencies provide a range of radial positions from the edge plasma to the core depending on plasma conditions. The system utilizes a combination of novel features to provide remote control of the probed density wavenumber, the launched polarization (X vs O-mode), and the angle of the launched DBS to match the magnetic field pitch angle. The range of accessible density turbulence wavenumbers (k_θ) is reasonably large with normalized wavenumbers $k_\theta \rho_s$ ranging from ≤0.5 to 9 (ion sound gyroradius ρ_s = 1 cm). This wavenumber range is relevant to a variety of instabilities believed to be important in establishing plasma transport (e.g., ion temperature gradient, trapped electron, electron temperature gradient, micro-tearing, kinetic ballooning modes). The system is specifically designed to address the requirement of density fluctuation wavevector alignment which can significantly reduce the SNR if not accounted for.

I. INTRODUCTION

Electron thermal transport in high power H-mode spherical tokamak (ST) plasmas generally far exceeds that due to collisional processes while, in contrast, the ion transport is found to be near the neo-classical collisional values (Refs. 1 and 2 and references therein). In spherical tokamaks, this anomalous electron thermal transport is often attributed to various instabilities including electron temperature gradient (ETG) modes, micro-tearing modes (MTM), global Alfvén modes (GAE), trapped electron modes (TEM), and kinetic ballooning modes (KBM). In comparison to conventional tokamaks, spherical tokamaks have reported a much stronger inverse scaling of confinement with collisionality ν^*.[3,4] This favorable scaling of energy confinement with collisionality has strong implications for reducing the size and costs of an ST based Component Test Facility. Measuring the level of density turbulence and flow velocities provides valuable insight into the turbulent processes that can affect confinement in fusion research devices. The density fluctuation level and flow velocity of plasma fluctuations can be measured using a technique termed Doppler backscattering (DBS) or Doppler reflectometry. This technique was pioneered by multiple researchers[5–8] and has since spread to many plasma devices around the world.[9–30] DBS is also being planned for the ITER tokamak.[13] From the range of references, it is evident that the technique has expanded both in the number of plasma devices as well as types of measurements including low and intermediate-k fluctuations, radial correlation lengths, GAMs, and zonal flows. It has also benefitted from theory and simulation attention.[31–42]

A new DBS system was installed and tested on the MAST-U spherical tokamak. The system launches eight simultaneous fixed

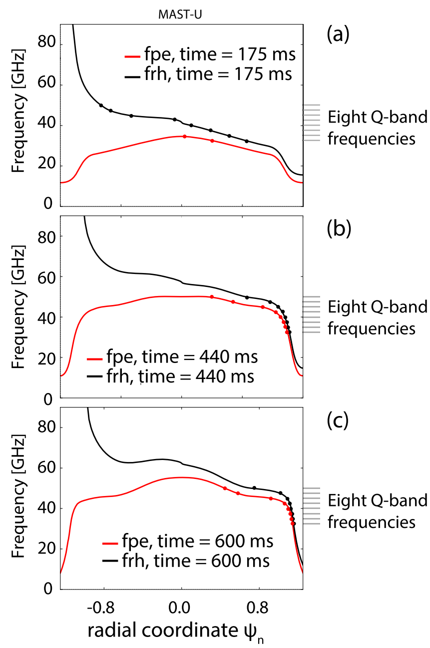

FIG. 1. Examples of radial access for the eight-channel Q-band DBS system on MAST-U. (a) Ohmic, (b) lower density H-mode, and (c) higher density H-mode.

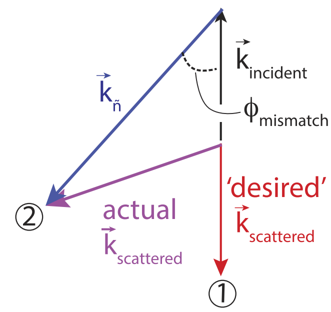

FIG. 2. Wavevector diagram illustrating an example of launch and scattered wavevectors. 1 and 2 are different receiver locations and the launch is at 1.

probe frequencies (32.5, 35, 37.5, 40, 42.5, 45, 47.5, and 50 GHz.) which all utilize the same optics. Figure 1 shows example radial coverage of this system for three different plasma confinement regimes: Ohmic, lower density H-mode, and higher density H-mode. The range of accessible density turbulence (ñ) wavenumbers (k_θ) is reasonably large with normalized wavenumbers $k_\theta \rho_s$ ranging from ≤0.5 to 9 (based upon 3D GENRAY[43] raytracing simulations and estimates of ion sound gyroradius ρ_s = 1 cm). This wavenumber range is relevant to a large variety of instabilities (e.g., ion temperature gradient, trapped electron, electron temperature gradient, micro-tearing, and kinetic ballooning modes).

II. SYSTEM DESIGN CONSIDERATIONS

The Doppler backscattering (often referred to as Doppler reflectometry) community has known from early on that the wavevector matching of the launched DBS beam as it relates to the so-called bi-normal direction of the density fluctuations can be critical to the operation of these systems. The bi-normal density wavevector is typically defined as the local vector that both lies in the flux surface and is perpendicular to the vector magnetic field **B**. The effect involves the geometries of the launch antenna, the receive antenna, and this bi-normal density fluctuation wavevector. This effect can be very significant, especially for a spherical tokamak, where the local magnetic pitch angle can be quite large. Figure 2 helps to illustrate the geometry of millimeter wave backscattering, the wavevectors involved, and the so-called mismatch angle, ϕ_{mismatch}. The figure shows the launch or incident wavevector, $\vec{k}_{incident}$; the desired backscattered wavevector, $\vec{k}_{scattered}$; and the density fluctuation wavevector, $\vec{k}_{\tilde{n}}$. The phrase "desired" backscattered wavevector is critical here and refers to the viewing geometry of the receiver. Although the density fluctuation wavevector $\vec{k}_{\tilde{n}}$ exists in the example of Fig. 2, it is not oriented in such a way as to scatter $\vec{k}_{incident}$ directly back to the receive antenna located at 1. Note that if a receiver was located at 2, it would receive a signal associated with $\vec{k}_{incident}$ and $\vec{k}_{\tilde{n}}$. The signal received by an antenna 1 will thus be reduced, potentially to the noise level, by the mismatch of the angle. The wavevector matching effect has been mathematically described[44] with the intensity signal written as

$$E^2 \sim \tilde{n}^2 e^{-0.5\left(k_{\tilde{n},x}-k_{scattered,x}\right)^2 a_x^2} e^{-0.5\left(k_{\tilde{n},y}-k_{scattered,y}\right)^2 a_y^2}. \tag{1}$$

The x and y directions are normal to the direction of propagation and E, $k_{\tilde{n},x}$, $k_{scattered,x}$, and a_x are the scattered electric field, the density fluctuation wavenumber in the x direction, the scattered wavenumber in the x direction, and the probe beam width in the x direction, respectively. The beam is assumed to have a Gaussian structure perpendicular to its direction of propagation. As can be seen, an analogous term for the y direction is also present. Taking the x direction as an example, relation (1) is interpreted as the power scattered into the wavenumber $k_{scattered,x}$ by the density fluctuations having a fluctuation wavenumber $k_{\tilde{n},x}$. The scattered intensity E^2 thus depends strongly on the wavenumber difference $k_{\tilde{n},x} - k_{scattered,x}$. If $k_{\tilde{n},x} - k_{scattered,x}$ is zero, this will result in the largest scattered signal and is referred to as the "matched" wavenumber condition. Using $k_{\tilde{n},x} = \left|\vec{k}_{\tilde{n}}\right| \sin\phi_{mismatch}$ and assuming that $k_{\tilde{n},y} - k_{scattered,y}$ is very nearly zero, (1) can be simplified[19]

$$E^2 \sim \tilde{n}^2 e^{-0.5 k_{\tilde{n}}{}^2 a_0^2 \sin^2(\phi_{mismatch})} \tag{2}$$

(also using the assumption that the probe beam is symmetric $a_x = a_y = a_0$). From (2), it is seen that the scattered power E^2 rapidly decreases as $k_{\tilde{n}}$ increases and that smaller $k_{\tilde{n}}$ are much less sensitive to $\phi_{mismatch}$ than higher $k_{\tilde{n}}$. (2) is a convenient simplification. Recent predictive modeling has shown a good ability to predict the mismatch response.[45]

Figure 3 illustrates this matching effect using experimental data where the received power is significantly reduced as the toroidal mismatch angle is increased (poloidal launch angle is constant). Figure 4 illustrates the required matching toroidal angle for a range of poloidal launch angles on MAST-U. These results were obtained using the GENRAY 3D[43] raytracing code. While not linear, the best

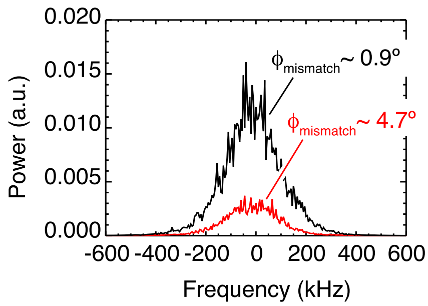

FIG. 3. Data from the DBS system on MAST-U illustrating nearly matched $\phi_{mismatch} \approx 0.9°$ and unmatched $\phi_{mismatch} \approx 4.7°$ conditions.

matching toroidal angle is seen to be roughly half of the poloidal launch angle. Scans such as these are used to optimize the DBS angles prior to taking plasma data. To perform this optimization, the magnetic equilibrium and density profiles used must be good estimates of the plasma shot to be measured. The ñ wavenumber to be monitored is then selected, and a range of toroidal launch angles is used in the GENRAY code from which the optimum toroidal angle is obtained. From this discussion, it is clear that a two-dimensional steering capability is essential for effective operation of DBS on MAST-U.

In the DBS design for MAST-U, this angular matching constraint is specifically dealt with by using a novel remotely adjustable lens/antenna arrangement. This provides the desired poloidal angle (determined by desired wavenumber to be probed) and required toroidal matching angles (as required to fully match the scattering wavevector, e.g., Fig. 4). Note that the DBS launch polarization will be matched to the MAST-U edge magnetic pitch angle via remotely controlled launch/receive antenna. In Secs. III and IV, it will be shown how the design and operation of the UCLA DBS/CPS systems took this wavevector matching effect and requirement explicitly into account.

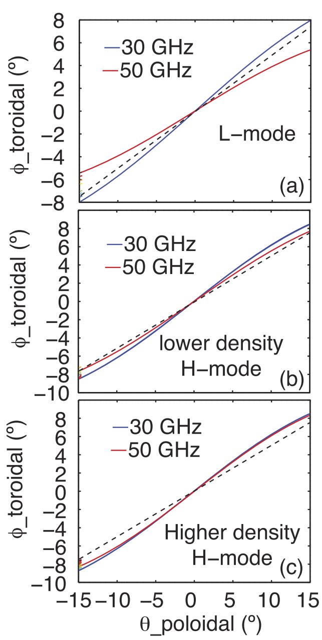

FIG. 4. Optimum toroidal launch angle vs poloidal launch angle and launch frequency from GENRAY 3D raytracing. For clarity, only 30 (slightly lower than the 32.5 GHz used in the system) and 50 GHz are shown for each condition. The dashed line is a reference using $\phi = 0.5\theta$. (a) L-mode, (b) lower density H-mode, and (c) higher density H-mode. Only X-mode right-hand cutoff results are shown.

III. SYSTEM DESIGN

For this project, UCLA utilized an existing eight channel Q-band DBS transmit and receive system (32.5–50 GHz). The design of this system is very similar to that shown in Peebles.[46] Due to the differences in frequencies between Peebles[46] and the Q-band system, different components were used; however, the overall circuit design remains analogous (specifics of this circuit and components used are available upon request). The DBS system is modular and designed to fit into a standard equipment rack (box size 22.9 × 43.2 × 43.2 cm^3) and easily transportable. The DBS data are acquired as quadrature signals, allowing the propagation direction, the Doppler shift magnitude, and the scattered power to be determined [E^2 in (1) or (2)]. Quadrature detection is a standard and powerful technique for DBS data acquisition. The Q-band system utilizes eight simultaneous probe frequencies 32.5, 35, 37.5, 40, 42.5, 45, 47.5, and 50 GHz that share the same optics and waveguides. Example radial locations using three different plasma regimes are shown in Fig. 1.

The MAST-U DBS system design incorporates several novel approaches that facilitate remote control operation. These include (a) remote selection of X-mode vs O-mode polarization, (b) remote tuning of the final polarization angle to match the edge pitch angle of the total magnetic field (for a given plasma and time), and (c) remote aiming control of launched probe and receive beams. Figure 5 illustrates the remote polarization selection utilizing two identical Q-band scalar antennas along with two remote controlled waveguide switches. Using O-mode DBS as an example [i.e., Fig. 5(a)], the eight probe frequencies are transmitted through waveguide switch No. 1, through the 3 dB directional coupler, to the O-mode antenna shown and then into the plasma. The signal from the plasma is received by the O-mode antenna and is directed to waveguide switch No. 2 by the 3 dB directional coupler and then to the receiver (not shown on the diagram). The X-mode DBS operation is analogous and is illustrated in Fig. 5(b). Note that with the circuit shown, the option of X-mode launch and O-mode received is possible [Fig. 5(c)] (and vice versa). This allows the system to be operated as a cross polarization scattering system capable of measuring internal magnetic fluctuations[47–49] (this option will not be discussed further in this article). The polarizer shown in Fig. 5(a) is a large aperture (25 cm diameter) parallel copper wires deposited on a Kapton polyamide film substrate that is mounted on a rotatable circular frame. The orientation of this frame and, thus, the polarizer are remote controlled, allowing selection of the final launch polarization. Due to the 45° tilt of the polarizer with respect to the beam [see Figs. 5 and 6(b)], the projection of the polarizer wires onto the beam must be taken into account when determining the polarizer angle,

$$\theta_{\text{polarizer}} = \mathrm{a}\tan(\tan(\theta_{\text{desired}})\cos(45°)), \quad (3)$$

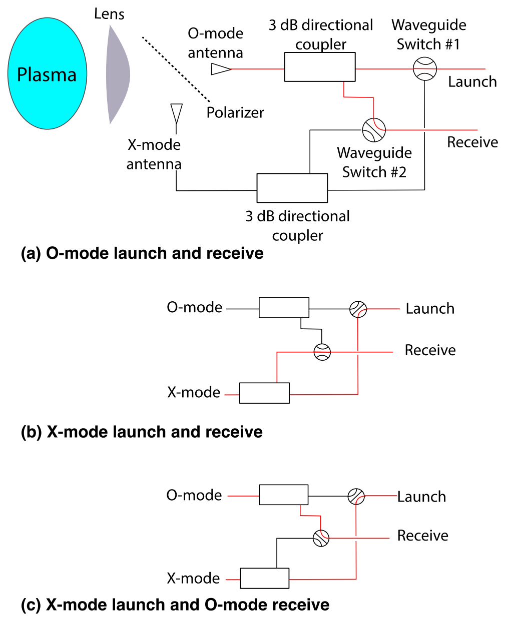

FIG. 5. Circuit diagram (not to scale) showing waveguide switches, couplers, polarizer, and lens for three different launch/receive configurations. Waveguides show example signal paths. Design allows for remote and independent switching of transmit and receive signals between O-mode (a), X-mode (b), or a combination (c).

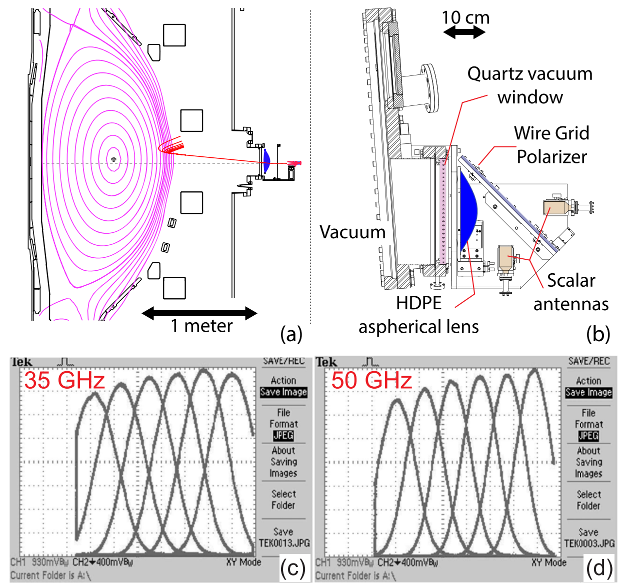

FIG. 6. (a) elevation view of MAST-U illustrating location of DBS system and beam steering and (b) plan view of showing location of various quasi-optical components. (c) and (d) beam profile laboratory data illustrating steering and beam quality of HDPE lens, taken 80 cm from lens, horizontal scale of 2 cm/div.

where $\theta_{desired}$ is the desired polarization angle of the beam as it enters the plasma and $\theta_{polarizer}$ is the polarizer angle setting.

During the design process, magnetic equilibria calculations indicated that MAST-U expected an average magnetic pitch angle of 36.4°. Taking into account the 45° polarizer frame tilt [Fig. 5 or Fig. 6(b) and Eq. (3)], this meant a static setting of 27.5° on the scalar antennas would provide the optimum starting point. The polarizer would then be adjusted around that angle in order to match the particular plasma being investigated. As an example, if the target plasma has an edge pitch angle of 38° (from magnetic equilibrium calculations), the polarizer would be rotated to a 28.9° setting on the polarizer frame. If we used X-mode in this example, there is a small amount of signal, with power proportional to $\sin^2(1.4°)$, that is not reflected by the polarizer and is rather transmitted through the polarizer. This unwanted radiation (O-mode polarization really) propagates upward [in reference frame of Fig. 5(a)] away from the plasma toward a beam dump. An analogous process occurs for O-mode, which transmits the required O-mode through the polarizer and reflects unwanted X-mode upward (Fig. 5).

The DBS poloidal and toroidal launch angles are selected using beam steering via horizontal and vertical movement of the lens (the lens is indicated in blue in Fig. 6). The angular range for the vertical and horizontal directions is 0–10.6°. These angular limits are set by size of the quartz vacuum window [Figs. 6(a) and 6(b)], the tube just inside the window, and to a lesser extent by structures inside the tokamak vacuum vessel [Fig. 6(a)]. The lens position is remotely set using two piezoelectric motors controlling the horizontal and vertical lens positions. Figure 6(a) diagrams how vertical beam steering would look, while Fig. 6(b) shows more of the details of the design including the polarizer, lens, and antenna placements. The piezomotors are located near the toroidal field coils and are completely non-magnetic to avoid any interaction with the MAST-U magnetic fields. Not indicated in Fig. 6(a) is the system's ability to independently steer toroidally and poloidally. The performance of this system was tested and optimized in the laboratory prior to installation on MAST-U. Figures 6(c) and 6(d) show laboratory beam profile measurements demonstrating the lens beam steering for two different frequencies, 35 and 50 GHz. The beam profiler is located 80 cm from the lens. As can be seen from the figure, the beam quality remains high as the angles change by ~8° [i.e., ~5.8 div * 2 cm/div = 11.6 cm, atan(11.6/80) ~ 8.3°].

IV. EXAMPLE PLASMA DATA

An example of the operation of the new DBS system is shown in Fig. 7. In that figure, both Ohmic and L-mode plasma phases are illustrated. Before the neutral beams at 300 ms, the mean Doppler frequency is slightly below zero for the 32.5 GHz channel [Fig. 7(d)] while the other two channels are somewhat symmetric around 0 kHz. After the neutral beam initiation, a delay of ~10 ms occurs before the three channels [Figs. 7(d)–7(f)] clearly respond. All channels show an increase toward positive frequencies with the higher probe frequencies showing larger changes. This Doppler shift variation is likely due to a radial variation of the local ExB velocity as the higher frequencies probe more deeply into the plasma and higher frequencies having a higher k with a larger Doppler shift (i.e.,

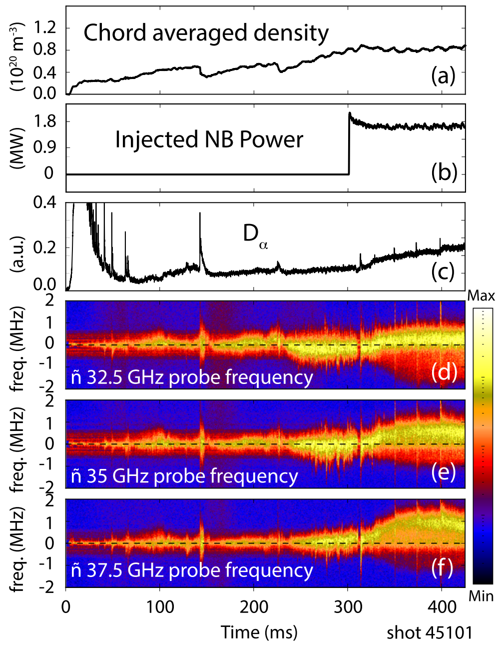

FIG. 7. Example MAST-U data with NB injection. DBS X-mode data from three probe frequencies (d)–(f). After the NBI starts near 300 ms, Doppler shifts are seen to rapidly change in the positive direction. Sawteeth oscillations also begin near 320 ms, which is seen on the signals (c)–(f). The ñ amplitudes plotted in (d)–(f) are log scales with respective min-max ranges of $(1.7 \times 10^{-5}, 0.08)$, (1.5–05, 0.09), and $(2.5 \times 10^{-5}, 0.11)$.

Doppler shift is given by $\Delta\omega = \vec{k} \cdot \vec{V}$). The system shows a high time resolution.

V. CONCLUSIONS

Toroidal and poloidal steering of the launched millimeter wave beam is known to be essential for effective use of DBS systems on a spherical tokamak. The DBS system on MAST-U specifically addresses this important requirement using a remotely controlled lens beam steering system. An innovative waveguide switching system is utilized to control the launch and receive polarizations (e.g., X-mode vs O-mode launch/receive). Finally, fine control of the polarization angle is achieved by a remotely controlled polarizer.

ACKNOWLEDGMENTS

This work supported by U.S. Department of Energy under Grant Nos. DE-SC0019005 and DE-SC0019007 and (part-) funded by the EPSRC Energy Programme (Grant No. EP/W006839/1).

AUTHOR DECLARATIONS

Conflict of Interest

The authors have no conflicts to disclose.

Author Contributions

T. L. Rhodes: Conceptualization (lead); Funding acquisition (lead); Investigation (equal); Methodology (equal); Project administration (lead); Resources (lead); Supervision (lead); Writing – original draft (lead); Writing – review & editing (lead). **C. A. Michael**: Investigation (equal); Software (equal); Validation (equal); Writing – original draft (equal). **P. Shi**: Data curation (equal); Investigation (equal); Software (equal). **R. Scannell**: Data curation (equal); Investigation (equal); Resources (equal). **S. Storment**: Formal analysis (equal); Methodology (equal); Software (equal). **Q. Pratt**: Formal analysis (equal); Investigation (equal); Methodology (equal). **R. Lantsov**: Conceptualization (equal); Investigation (equal); Methodology (equal). **I. Fitzgerald**: Conceptualization (equal). **V. H. Hall-Chen**: Formal analysis (equal); Investigation (equal). **N. A. Crocker**: Formal analysis (equal); Investigation (equal); Software (equal). **W. A. Peebles**: Conceptualization (equal); Investigation (equal); Methodology (equal).

DATA AVAILABILITY

The data that support the findings of this study are available from the corresponding author upon reasonable request.

REFERENCES

[1] H. Meyer *et al.*, Nucl. Fusion **49**, 104017 (2009).
[2] J. E. Menard *et al.*, Nucl. Fusion **52**, 083015 (2012).
[3] S. M. Kaye *et al.*, Nucl. Fusion **47**, 499–509 (2007).
[4] M. Valovic *et al.*, Nucl. Fusion **51**, 073045 (2011).
[5] V. V. Bulanin, D. O. Korneev, V. A. Rozhansky, and M. Tendler, *Contact Papers, Part II* (Bournemouth, 1995), Vol. 19c, pp. 089–092.
[6] X. L. Zou *et al.*, in *26th EPS Conference on Controlled Fusion and Plasma Physics, Maastricht, 14–18 June 1999* (ECA, 1999), Vol. 23J, pp. 1041–1044.
[7] M. Hirsch *et al.*, Plasma Phys. Controlled Fusion **43**, 1641 (2001).
[8] G. D. Conway, J. Schirmer, S. Klenge, W. Suttrop, E. Holzhauer, and ASDEX Upgrade Tea, Plasma Phys. Controlled Fusion **46**, 951–970 (2004).
[9] V. V. Bulanin *et al.*, Plasma Phys. Rep. **26**, 813 (2000).
[10] G. D. Conway *et al.*, Plasma Phys. Controlled Fusion **47**, 1165 (2005).
[11] J. Schirmer *et al.*, and ASDEX Upgrade Team, Nucl. Fusion **46**, S780 (2006).
[12] E. Z. Gusakov *et al.*, Plasma Phys. Controlled Fusion **48**, B443 (2006).
[13] G. Vayakis *et al.*, Nucl. Fusion **46**, S836–S845 (2006).
[14] P. Hennequin *et al.*, Nucl. Fusion **46**, S771–S779 (2006).
[15] J. Schirmer *et al.*, Plasma Phys. Controlled Fusion **49**, 1019 (2007).
[16] T. Happel *et al.*, Rev. Sci. Instrum. **80**, 073502 (2009).
[17] T. Estrada *et al.*, Plasma Phys. Controlled Fusion **54**, 124024 (2012).
[18] L. Schmitz *et al.*, Phys. Rev. Lett. **108**, 155002 (2012).
[19] J. C. Hillesheim *et al.*, Nucl. Fusion **55**, 073024 (2015).
[20] T. Estrada *et al.*, Nucl. Fusion **61**(4), 046008 (2021).
[21] T. Happel *et al.*, Plasma Sci. Technol. **22**, 064002 (2020).
[22] P. Hennequin *et al.*, in 2nd Asia-Pacific Conference on Plasma Physics (AAPPS-DPP 2018), 2018.
[23] K. Höfler *et al.*, Plasma Phys. Controlled Fusion **63**, 035020 (2021).
[24] J. Jiaxu *et al.*, Plasma Sci. Technol. **23**, 095106 (2021).
[25] P. Molina Cabrera *et al.*, Rev. Sci. Instrum. **89**(8), 083503 (2018).
[26] J. R. Pinzón *et al.*, Plasma Phys. Controlled Fusion **61**(10), 105009 (2019).
[27] X. H. Ren *et al.*, Rev. Sci. Instrum. **92**(3), 033545 (2021).
[28] T. L. Rhodes *et al.*, Rev. Sci. Instrum. **89**, 10H107 (2018).
[29] T. Tokuzawa *et al.*, Rev. Sci. Instrum. **89**, 10H118 (2018).
[30] A. Y. Yashin *et al.*, J. Instrum. **17**(01), C01023 (2022).

[31] L. G. Bruskin *et al.*, Plasma Phys. Controlled Fusion **46**, 1313–1330 (2004).
[32] E. Z. Gusakov and A. V. Surkov, Plasma Phys. Controlled Fusion **46**, 1143 (2004).
[33] E. Z. Gusakov, A. V. Surkov, and A. Y. Popov, Plasma Phys. Controlled Fusion **47**, 959–974 (2005).
[34] E. Blanco, T. Estrada, and J. Sánchez, Plasma Phys. Controlled Fusion **48**, 699 (2006).
[35] V. V. Bulanin and M. V. Yafanov, Plasma Phys. Rep. **32**(1), 47–55 (2006).
[36] C. Lechte, IEEE Trans. Plasma Sci. **37**, 1099 (2009).
[37] T. Happel, E. Blanco, and T. Estrada, Rev. Sci. Instrum. **81**, 10D901 (2010).
[38] O. L. Krutkin *et al.*, Nucl. Fusion **59**(9), 096017 (2019).
[39] J. R. Pinzon, Ph.D. thesis, Technische Universität München and Universidad Carlos III de Madrid, 2018.
[40] J. R. Ruiz *et al.*, Plasma Phys. Control. Fusion **64**, 055019 (2022).
[41] V. Hall-Chen, Ph.D. thesis, University of Oxford, 2022.
[42] V. Hall-Chen, F. I. Parra, and J. Hillesheim, Plasma Phys. Control. Fusion **64**, (2022) .
[43] A. P. Smirnov *et al.*, in *Proceedings of 15th Workshop on ECE and ECRH* (Singapore World Scientific, 2009), p. 301, www.compxco.com/genray.html.
[44] R. E. Slusher and C. M. Surko, Phys. Fluids **23**, 472 (1980).
[45] V. H. Hall-Chen *et al.*, Rev. Sci. Instrum. **93**, 103536 (2022).
[46] W. A. Peebles, T. L. Rhodes, J. C. Hillesheim, L. Zeng, and C. Wannberg, Rev. Sci. Instrum. **81**, 10D902 (2010).
[47] X. L. Zou *et al.*, Phys. Rev. Lett. **75**, 1090 (1995).
[48] T. Lehner, J. M. Rax, and X. L. Zou, Europhys. Lett. **8**, 759 (1989).
[49] L. Vahala, G. Vahala, and N. Bretz, Phys. Fluids B **4**, 619 (1992).